Genetic Analysis of Vertebrate Sensory Hair Cell Mechanosensation: the Zebrafish Circler Mutants

Teresa Nicolson,*# Alfons Rüsch,‡
Rainer W. Friedrich,† Michael Granato,*‖
Johann Peter Ruppersberg,‡§
and Christiane Nüsslein-Volhard*
*Max-Planck-Institut für Entwicklungsbiologie
Spemannstrasse 35 Abteilung Genetik
†Abteilung Physikalische Biologie
‡Physiologisches Institut
Gmelinstrasse 5
§Sektion Sensorische Biophysik
Hals-Nasen-Ohren Klinik Röntgenweg 11
Eberhard-Karls-Universität Tübingen
72076 Tübingen
Federal Republic of Germany
‖University of Pennsylvania
Department of Cell and Developmental Biology
Philadelphia, Pennsylvania 19104

Summary

The molecular basis of sensory hair cell mechanotransduction is largely unknown. In order to identify genes that are essential for mechanosensory hair cell function, we characterized a group of recently isolated zebrafish motility mutants. These mutants are defective in balance and swim in circles but have no obvious morphological defects. We examined the mutants using calcium imaging of acoustic-vibrational and tactile escape responses, high resolution microscopy of sensory neuroepithelia in live larvae, and recordings of extracellular hair cell potentials (microphonics). Based on the analyses, we have identified several classes of genes. Mutations in *sputnik* and *mariner* affect hair bundle integrity. Mutant *astronaut* and *cosmonaut* hair cells have relatively normal microphonics and thus appear to affect events downstream of mechanotransduction. Mutant *orbiter*, *mercury*, and *gemini* larvae have normal hair cell morphology and yet do not respond to acoustic-vibrational stimuli. The microphonics of lateral line hair cells of *orbiter*, *mercury*, and *gemini* larvae are absent or strongly reduced. Therefore, these genes may encode components of the transduction apparatus.

Introduction

Physical motion and sound are detected by sensory hair cells. Vertebrate hair cells, as other sensory cells, are thought to have evolved from a common ciliated ancestral cell (reviewed by Popper et al., 1992). The apical bundle of actin-filled stereocilia is the site of specialization for mechanosensitive transduction (reviewed by Hudspeth, 1989; Ashmore, 1991; Corwin and Warchol, 1991). Each bundle contains up to 300 stereocilia arranged in increasing height. The stereocilia are linked to each other by very fine extracellular lateral and oblique

filaments (Bagger-Sjöbäck and Wersäll, 1973; Osborne et al., 1984; Little and Neugebauer, 1985). The current model of hair cell mechanotransduction, the "gating-spring" hypothesis, is based on a number of sophisticated experiments conducted over the last decade. It is thought that the fine filaments, known as "tip links," are directly connected to transduction channels and act like springs that tug open or gate the channels during mechanical shearing of the stereocilia (Corey and Hudspeth, 1983; Pickles et al., 1984; Assad et al., 1990; reviewed by Gillespie, 1995). The influx of cations such as K^+ and Ca^{2+} causes depolarization of the cell, activating voltage-sensitive channels and causing subsequent neurotransmitter release. An alternative model for transduction hypothesizes that the cilium-to-cilium membrane junctions also observed near the tips are involved in stretching the membrane and thus activating mechanosensitive membrane channels (Thurm, 1981; reviewed by Hackney and Furness, 1995). Despite the immense progress in recent years on mechanosensitive hair cells of vertebrates, there is a stark discrepancy between the biophysical and molecular analyses of mechanotransduction. Although the physiological characterization of the auditory mechanosensitive transduction channel has lead to an elaborate gating-spring model of transduction, little progress has been achieved in identifying essential components of the transduction apparatus. Progress in this area would be of great benefit since most cases of congenital deafness are due to defects within the neuroepithelium (reviewed by Brown and Steel, 1994).

The molecular analysis of the mechanoelectrical transduction apparatus is hampered by one main disadvantage: the extreme scarcity of material. Each hair cell contains presumably only 100 copies of the transduction channel (Howard and Hudspeth, 1988; Denk et al., 1995), making a biochemical approach extremely difficult. However, a genetic approach appears to be more promising. The recent positional cloning of the mouse *Shaker1* and *Snell-waltzer* genes has identified two unconventional myosins that are essential for normal hair cell morphology and function (Avraham et al., 1995; Gibson et al., 1995). Additional support comes from saturation screens performed in *Caenorhabditis elegans* and *Drosophila melanogaster* to identify genes involved in mechanosensation. In *C. elegans*, a behavioral screen based on a touch avoidance reaction has led to the identification of several genes required for mechanotransduction (reviewed by Hamill and McBride, 1996; Tavernarakis and Driscoll, 1997). Many of the *C. elegans* MEC (mechanosensory abnormality) genes have been cloned and sequenced. They encode extracellular matrix components such as MEC-9, an agrin-like protein that may be attached to the transduction apparatus (Du et al., 1996). Degenerin ion channel subunits MEC-4 and MEC-10, which are related to the amiloride-sensitive epithelial sodium channel superfamily, are likely to form mechanosensitive channels (Driscoll and Chalfie, 1991; Huang and Chalfie, 1994). Cytoskeletal components such as stomatin (MEC-2) and tubulin subunits (MEC-7

Table 1. Mutations affecting larval vestibular function

Gene	Abbreviation	n	Alleles
sputnik*	spu	5	te370e^j, tz300a, tc242b, tj264a, tc317e
mariner*	mar	3	tc320b, tr202b, ty220d
orbiter*	orb	2	tc256e^f, th263b
mercury	mrc	1	tk256c
gemini	gem	1	tc323d
skylab	skb	1	tm246a
astronaut	asn	1	tm290d
cosmonaut	csm	1	tr279a^f

*Different strengths among alleles; ^{j}viable allele; ^{f}semi-viable allele.

and MEC-12) may be associated with the transduction channel (Savage et al., 1989; Huang et al., 1995). In Drosophila, two behavioral screens for larval touch insensitivity and adult uncoordination have uncovered seven genes that affect transduction (Kernan et al., 1994). The cloning and sequencing of the fly genes may also reveal a similar set of components required for mechanotransduction.

This study takes advantage of a vertebrate genetic system, that of the zebrafish. In a large-scale screen for behavioral locomotive defects, over 150 motility mutants were identified, including a number of mutants with defects in balance (Granato et al., 1996). The inability to maintain balance is indicative of defects within the mechanosensory organs of the auditory-vestibular system. In contrast to zebrafish developmental ear mutants that have obvious morphological defects (Malicki et al., 1996; Whitfield et al., 1996), the gross morphology of the inner ear is normal in the circler mutants. Here we classify the circlers based on physiology and morphology of the sensory neuroepithelium of the inner ear and lateral line system. Behavioral tests show that the majority of circler mutants can detect tactile stimuli, but cannot detect acoustic/vibrational stimuli or gravitational stimuli. Physiological analysis demonstrates that the defects are peripheral and in some cases the sensory hair cells lack microphonics, the extracellular voltage component of the primary transduction event. Thus, the zebrafish circlers permit genetic dissection of the transduction mechanism in vertebrate sensory hair cells.

Results

Behavioral Defects in Zebrafish Circlers

During a recent large-scale mutagenesis screen, a large number of homozygous recessive motility mutants were isolated, including 15 morphologically normal mutants with defective balance (Granato et al., 1996). Complementation analysis shows that these 15 mutants fall into eight groups (Table 1). For three genes, two or more

alleles have been isolated, whereas the remaining five mutants are single alleles. Many of the mutations are lethal, with larvae surviving until day 8. The vestibular defects among these mutants become apparent on day 3. At this stage, the larvae fail to maintain an upright position in contrast to wild-type siblings. When touched in the head or tail region, mutant larvae exhibit an escape response, although they swim on their sides or back and often land on their heads. In contrast to tactile stimuli, the majority of the nonviable mutants do not respond to vibrational stimuli (tapping on the petri dish). On days 4 and 5, circular movements, including both looping and rolling motions, become more obvious. On day 5 or later, many develop an upward curved spine, which enhances the circling behavior. Nonviable mutants tend to be less active than their wild-type siblings and also fail to develop an air-filled swim bladder, which may account for the lethality. Many of the lethal alleles cause a similar, if not identical, behavioral phenotype.

The absence of an air-filled swim bladder is common among zebrafish motility mutants and also among other types of zebrafish mutants such as pigment and jaw mutants (Granato et al., 1996, Haffter et al., 1996). An air-filled larval swim bladder does not appear to be necessary for detection of acoustic-vibrational stimuli since the jaw, pigment, and other swim bladder–less mutants respond to such stimuli (unpublished data), and therefore its absence is unlikely to be the cause of larval behavioral defects present in the circlers. Nevertheless, it is unclear why the swim bladder does not fill with air. The failure to fill the swim bladder with air in the nonviable mutants, as in other motility mutants, may be the cause of death since the larvae in all cases are unable to swim to the surface to feed. Alternatively, the circler gene products may be required for other functions essential for survival.

The genes sputnik, cosmonaut, and orbiter have homozygous viable alleles that cause a recessive adult phenotype. The viable larvae have air-filled swim bladders, but 25% or less survive to adulthood. Many larvae die within 14 days, especially those with severe postural defects (floating continually upside down or sideways)
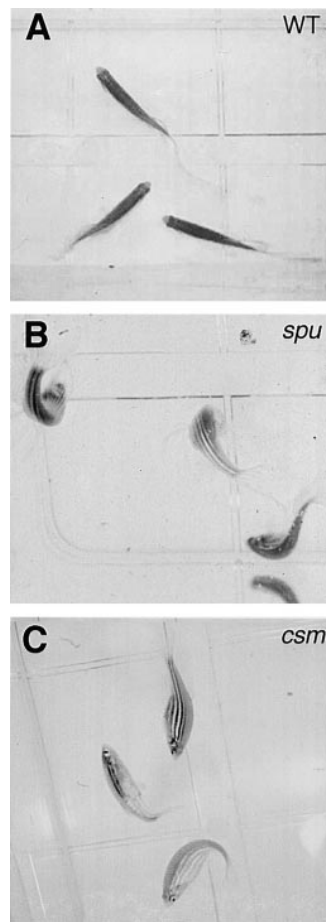
Figure 1. Dorsal View of the Swimming Patterns of Adult Wild-Type and Mutant *sputnik* and *cosmonaut* Fish

(A) Wild-type fish maintain a normal position with respect to their dorsoventral axis. Their lateral stripes are rarely seen from above.
(B) *sputnik* fish exhibit spontaneous head-forward ventral and lateral looping patterns of swimming (allele *te370e*). During this frame, all three fish had their heads facing the bottom of the tank. In general, *sputnik* fish circle around a point outside of the body.
(C) *cosmonaut* fish spin in a pinwheel fashion around an axis centered near the head (allele *tr279a*). This mutant tends to swim at a tilt, keeping either side facing downward, perpendicular to the bottom of the tank.

that presumably have difficulty in feeding. The defect in balance appears on day 4 or 5, and the phenotype is variable. Some larvae make looping movements similar to the nonviable mutants, while others have a more subtle phenotype of swimming at a tilt or resting with their head oriented downward. The viability and variable phenotype suggest that these alleles of *sputnik* and *orbiter* are weaker alleles. The *cosmonaut* mutation causes a similar larval swimming pattern, but in contrast, all *cosmonaut* larvae are sensitive to vibrational stimuli. The adult phenotype of the viable mutants also varies in severity between individuals. The circling behavior of mutant *sputnik* adults consists mainly of forward somersaulting and random lateral looping (Figure 1B). Animals homozygous for *orbiter* rarely survive, but those that do exhibit lateral looping behavior similar to *sputnik* adults.

Thus, *sputnik* and *orbiter* adult fish mimic the behavior of fish under micro- or zero-gravity conditions (von Baumgarten et al. 1975) and fish that have undergone lesions or removal of the vestibular organ (Pfeiffer, 1964). Mutant *cosmonaut* adults, in contrast, spin around an axis centered near the head and mimic the motion of a pinwheel (Figure 1C).

Potentiated Dorsal Light Reflex Indicates Loss of Vestibular Function

Equilibrium orientation in fish involves both an optic and static or gravitational component (von Holst, 1935). The dorsal light reflex is the natural inclination to orient the dorsal side toward light. A fish illuminated from the side will shift its dorsoventral axis from the vertical plane down to an angle of 40° or less, depending on the species and whether the animal was preadapted to darkness (von Holst, 1935, 1950). The static component prevents the fish from making any further adjustments. To determine whether the vestibular system can function in adult viable circler mutants, we tested the dorsal light reflex. *sputnik* mutants instantaneously adopted an angle of approximately the same degree, keeping their dorsal side turned toward the light source while swimming along the side of their cage (Figure 2B). Identical results were obtained with mutant *orbiter* adults (data not shown). In contrast, there was no immediate significant effect on the wild-type fish (Figure 2A). This is an expected result since the dorsal light reflex is normally gradual and dependent on preadaptation to darkness (von Holst, 1935). Mutant *cosmonaut* fish behaved like wild-type fish with no striking change of orientation upon exposure to the lateral light source (data not shown). The potentiated dorsal light reflex along with the swimming behavior support the hypothesis that mutant *sputnik* and *orbiter* fish do not sense gravity, whereas mutant *cosmonaut* fish still retain this ability.

Absence of the Acoustic/Vibrational Startle Reflex

When raised at 30°C, we observe that zebrafish larvae begin to adopt an upright position at 72 hr, before the swim bladder fills with air. At 76 hr, spontaneous short bursts of swimming may occur. The swim bladder fills with air around 96 hr, and swimming becomes more frequent and includes more complex movements. The acoustic/vibrational startle reflex occurs in response to water-borne vibrations. Tapping a petri dish on the rim causes a quick escape reaction in the larvae that results in displacement by a full body length or more (Kimmel et al., 1974). In adult teleost fish such as *Danio rerio*, the swim bladder, which is coupled to the endolymph of the inner ear via a series of bones, increases sensitivity to acoustic stimuli (reviewed by Popper and Platt, 1993). We find that the swim bladder may not be necessary for larval auditory sensitivity since the acoustic/vibrational escape response is present in 72 hr larvae before the swim bladder fills. In addition, there is some overlap in frequency sensitivity between the inner ear and a second mechanosensitive organ found in lower vertebrates, the lateral line system (Popper and Platt, 1993). Thus, any low frequency components of the tapping stimulus (visible as waves across the surface) may also stimulate the lateral line organ.
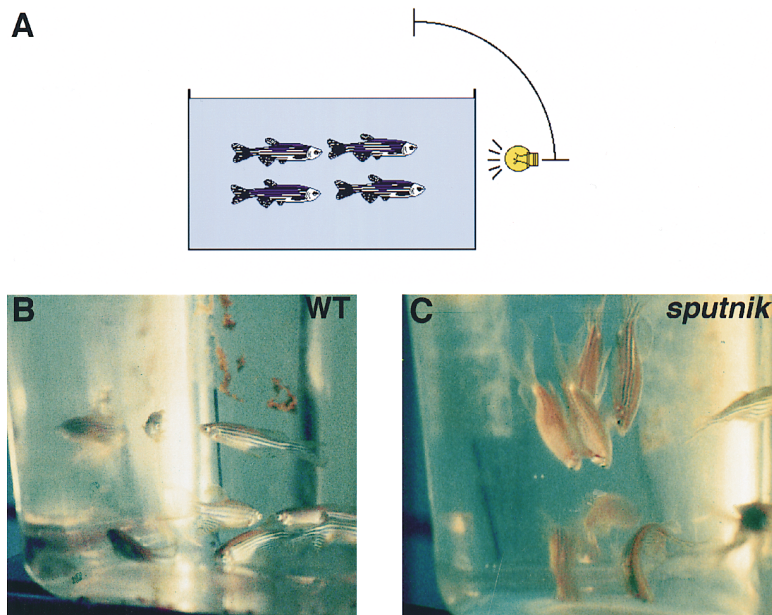
A

B WT

C *sputnik*

Figure 2. Potentiated Dorsal Light Reflex in Adult *sputnik* Animals

(A) Fish were placed in a dark room and illuminated from the side as schematically shown.

(B) Wild-type fish did not significantly shift their dorsoventral axis during illumination.

(C) *sputnik* fish instantaneously adopted a new angle of inclination or orientation in response to illumination. The majority of mutants shifted their dorsoventral axis by ∼90° and swam along the side of the tank as if it were the bottom of the cage. All mutant *sputnik* adults tested exhibited a potentiated response regardless of the variability of their phenotype. However, those fish with a weaker phenotype tended to have a less potentiated response and spent more time swimming in other areas of the tank.

The acoustic-vibrational startle reflex is a quick response that involves a relatively simple neural circuit (reviewed by Korn and Faber, 1996). The sensory hair cells of the otolithic organs and lateral line system activated by auditory or vibrational stimuli cause the firing of the primary neurons of the eighth nerve or lateral line nerve ganglia that directly and indirectly activate the Mauthner cells. The Mauthner cells in turn activate motor neurons, resulting in the contraction of muscle fibers. Mauthner cells are also activated by sensory neurons that detect touch.

With the exception of *cosmonaut*, *skylab*, and the weaker alleles of *sputnik* and *orbiter*, the nonviable mutants do not respond to a vibrational tapping stimulus (Table 2; n >10 for each allele). In order to locate the defect in acoustic-vestibular function, we monitored neuronal activity in the mid- and hindbrain by calcium imaging of 5-day-old larvae. Neurons in this region, which include the Mauthner cells, are activated in response to vibration as well as touch. If the mutants have specific defects in detecting sound and/or vibration, we expected that mid- and hindbrain neurons would be silent in response to such stimuli. However, tactile stimuli, which activate other sensory neurons, should still be effective in eliciting responses.

In all preparations of wild-type larvae tested (63 stimulations, n = 13), vibrational stimuli elicited prominent changes in fluorescence in the mid- and hindbrain (Figures 3B and 3D). Between individuals, the spatial pattern of fluorescence change showed some variability, presumably due to small differences in the orientation of the preparations, the focal plane, and the labeling intensity. However, gross features of activity patterns were constant across animals in the regions around and anterior to the ear and the presumptive positions of the Mauthner cell and its serial homologs. The time course of the calcium signal was transient and clearly correlated with
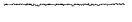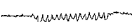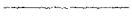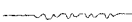
the stimulus (Figure 3D). Calcium signals were also observed in response to weak stimuli that did not elicit escape movements. Since previous experiments (O'Malley et al., 1996) have shown that escape movements are correlated with a calcium signal in the Mauthner cell in an all-or-none fashion, some of the calcium signals observed originate at least in part from interneurons other than the Mauthner cell and its homologs.

In contrast to wild-type larvae, no calcium signals were observed in response to vibrational stimuli in most of the nonviable mutants. For example, mutant *sputnik* larvae failed to show a calcium response (Figures 3F and 3H; 44 stimulations, n = 10; allele *tz300a*). Significant responses were observed only in mutant *cosmonaut* and *skylab* larvae. In these mutants, the overall intensity of the calcium signals was reduced compared to wild type, but the spatial pattern o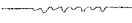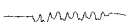f calcium signals was not grossly different from wild type (Figures 3K and 3M). However, small differences in the pattern of activity may not have been detected because of the considerable degree of variability between preparations.

Examination of the time courses of the relative change in fluorescence ($\Delta F/F$) in the mid/hindbrain region indicates that stimulus-induced responses are clearly present in mutant *cosmonaut* and *skylab* larvae, although reduced in magnitude (Figure 3M). The response in *skylab* is not transient but lasts considerably longer than responses in wild-type and *cosmonaut* larvae.

In order to compare quantitatively the calcium responses, we determined the mean peak signal within the stimulation period (5 taps within 3 s) for each stimulus presentation (Table 2). Mutants that show no behavioral response to vibrational stimuli (*mercury* [32 stimulations, n = 6], *orbiter* [38 stimulations, n = 5], *gemini* [36 stimulations, n = 7], *sputnik* [44 stimulations, n = 10], *mariner* [17 stimulations, n = 5], and *astronaut* [28 stimulations, n = 6] larvae) do not display calcium signals or display only very small signals. In contrast, mutant *cosmonaut*

Table 2. Summary of the phenotypes of the vestibular mutants

| Strain	Allele	Hair cell morphology	Acoustic Vibrational Sensitivity[¥]	Startle reflex Ca²⁺ signal (%)	Microphonic potentials (µV)	
Wild type		normal	+	100± 56	17.0 ± 6.4	
Class I:						
skylab (skb)	tm246a	degeneration	±	51 ± 32	n.d.	n.d.
Class II:						†
sputnik (spu)	tz300a	bundle defect	—	0 ± 7	0	
	tc242b	"	—	n.d.	0	
	tc317e	"	—	n.d.	0	
						†
	te370e*	"	±	n.d.	5.5 ± 1.6	
mariner (mar)	tc320b	bundle defect	—	9 ± 8	0	
	ty220d	"	—	n.d.	0	
	tr202b	"	—	n.d.	4.5 ± 3.4	
Class III:						
mercury (mrc)	tk256c	normal	—	0 ± 8	0	
orbiter (orb)	th263b	normal	—	4 ± 8	0	
	tc256e*	"	±	n.d.	4.7 ±1.7	
gemini (gem)	tc323d	normal	—	3 ± 10	4.8 ± 2.2	
Class IV:						
astronaut (asn)	tm290d	normal	—	14 ± 16	12.3 ± 3.2	
Class V:						
cosmonaut (csm)	tr279a*	normal	+	42 ± 35	19.2 ± 2.7	

*Viable alleles
[¥]Observed behavior; + indicates wild type sensitivity, ± indicates partial sensitivity, and - indicates no sensitivity
[†]tz300a and te370e were stimulated by a sine wave of 40 Hz, 8 cycles, all other alleles by 20 Hz, 4 cycles. For all mutants, between 3 and 8 animals were tested. Records are averages of 200 presentations. Neuromasts were stimulated by a fluid jet and potentials were measured peak to peak.

and skylab larvae, which exhibit either an intact or partial startle reflex, had calcium signals that were reduced to 42% ± 35% and 51% ± 32% (mean ± SD) of wild type, respectively.

The lack of calcium signal in mid- and hindbrain neurons in response to vibrational stimuli could reflect a defect intrinsic to mid- and hindbrain neurons or one arising in the periphery. In order to distinguish between these possibilities, we tested the calcium response to tactile stimuli to the forehead, which is innervated by the somatosensory cranial nerves; these nerves activate the hindbrain and spinal cord circuitry involved in both acoustic and touch-induced startle reflexes. In wild-type larvae (22 stimulations, n = 5), touch stimuli induced calcium signals comparable in magnitude to those induced by vibrational stimuli. Within the same preparation, the spatial pattern of fluorescence change depended on the exact location of the stimulus. However, in the regions ventral and just posterior to the eye corresponding to the position of the trigeminal ganglion and around the presumed positions of the Mauthner cell and its homologs, calcium responses were always present. As illustrated in Figures 3G and 3H for sputnik, touch stimuli also induced calcium signals in all of the mutants tested (mercury [5 stimulations, n = 2], orbiter [12 stimulations, n = 4], gemini [n.d.], sputnik [51 stimuli, n = 11], mariner [6 stimulations, n = 2], astronaut [10 stimulations, n = 2] cosmonaut [25 stimulations, n = 7], and
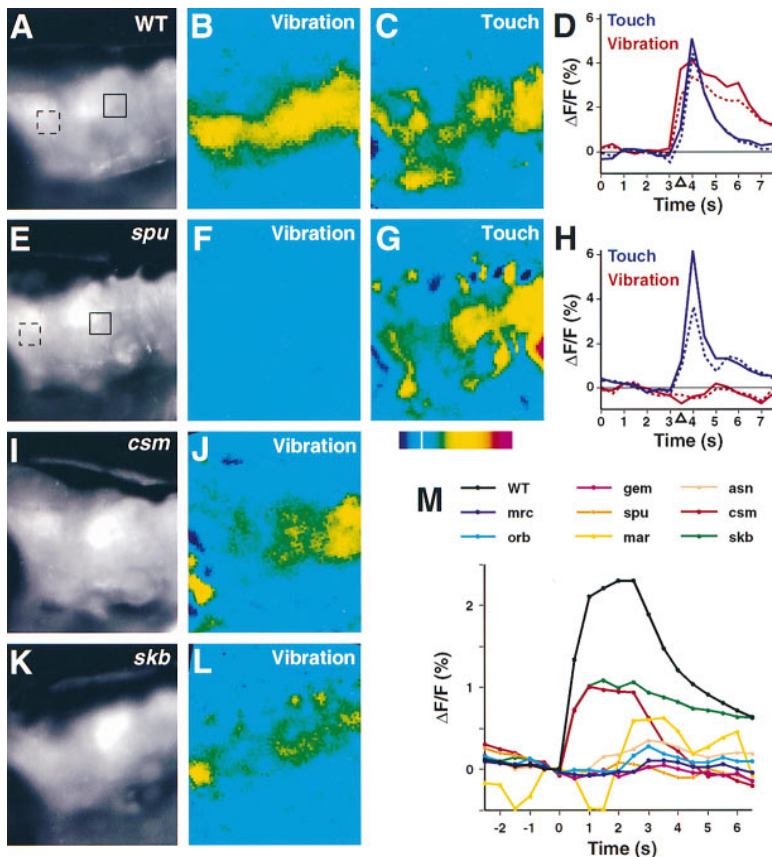
Figure 3. Calcium Imaging of Touch-Induced and Acoustic-Vibrational Escape Responses in Day 5 Larvae

Whole animals were labeled with the calcium indicator Calcium Green-1 dextran by injection of the dye into one to four cell blastulae. For imaging, larval preparations were embedded in low-melting agarose and viewed from the side.

(A, E, I, and K) Raw fluorescent images of Calcium Green-1 dextran labeling in the midbrain/hindbrain region in a wild type (A), *sputnik* ([E], allele *tz300a*), (I) *cosmonaut*, and (K) *skylab* larvae, respectively. The plane of focus is slightly medial to the posterior otolith, which is still visible.

(B–C, F–G, J, and L) Color coded images of the relative change in fluorescence in response to a touch or vibrational stimulus. Color scale indicates the relative change in fluorescence ($\Delta F/F$) from -2.5% (black) to 10% (red). Zero change is indicated by the white line. (B) and (C) are from the same view as (A); (F) and (G) are from the same view as (E); (J) is from the same view as (I); (L) is from the same view as (K).

(B, J, and L) Activity induced by a vibrational stimulus in wild-type, *cosmonaut*, and *skylab* larvae, respectively.

(F) Absence of a response to a vibrational stimulus in a mutant *sputnik* larva.

(C and G) Changes in fluorescence induced by a touch stimulus on the forehead in wild-type and *sputnik* larvae, respectively. Time courses of calcium responses are shown in (D) (wt) and (H) (*sputnik*). The solid line shows the time course of fluorescence change in the region indicated by the solid box, which is in the posterior region near the location of the Mauthner cell. The dotted line depicts the time course in the region indicated by the dotted box, which is near the ventral region of the optic tectum. These areas (outlined by boxes) were chosen for quantitation since they appear to undergo the greatest change in fluorescence.

(M) Time course of the responses to vibrational stimuli in wild-type and mutant larvae. The vibrational stimuli were delivered at time point 0, over a period of 3 s. Each time point is the average peak value of the $\Delta F/F$ in the mid- and hindbrain region determined from many trials with several preparations. Delayed and very small responses were observed in some mutants, especially *astronaut*, although their degree of significance is less clear. The high variability in the time course observed in mutant *mariner* larvae was due to spontaneous activity in the absence of stimulation.

skylab [13 stimulations, n = 4]; data not shown). The neural circuitry mediating the escape reflex to tactile stimuli therefore appears to be normal in the circlers.

Our analysis indicates that the circler mutants respond to tactile stimuli but show reduced or absent response to vibration stimuli. The absence of vibration-induced calcium signals in mutant larvae suggest that the first-order interneurons are not being activated. The molecular defect in the mutants is most likely located peripherally, either in the eighth nerve or mechanosensory hair cells.

Gross and Fine Structure of the Inner Ear in Circler Larvae

The structure of the inner ear vestibule and ultrastructure of mechanosensory hair cells is conserved among vertebrates, including *Danio rerio*. A major advantage of using zebrafish as a model system is the transparency of larvae. The canals and otolithic structures of the inner ear are readily visible. By 72 hr, otocysts contain three semicircular canals with corresponding cristae and two otolithic endorgans or maculae (Haddon and Lewis, 1996). Later in juvenile fish, otocysts divide up into the pars superior, containing the utricle and semicircular canals, and the pars inferior, which consists of the saccule, lagena, and macula neglecta (Platt, 1993; Haddon and Lewis, 1996). In all mutants, the gross structure of the otocysts appears to be normal with respect to canal structures, ototliths, and sensory hair cell patches (Figure 4A and data not shown).

Each semicircular canal contains a crista, or cluster of about 20 hair cells, which is coupled to a gelatinous cupula spanning the canal. At high magnification, the long kinocilia (up to 25 μm) and stereociliary bundles (up to 5 μm) of semicircular canal hair cells are visible in live, intact larvae (Figure 4B, wild type, dorsal view of posterior canal). We examined all available alleles and found several with neuroepithelial defects. Hair cell bundle defects are present in *mariner* and *sputnik* (Figures 4C and 4D, respectively). In both mutants, the stereociliary bundles appear to be detached from the kinocilia, and in some cases the stereocilia appear to be
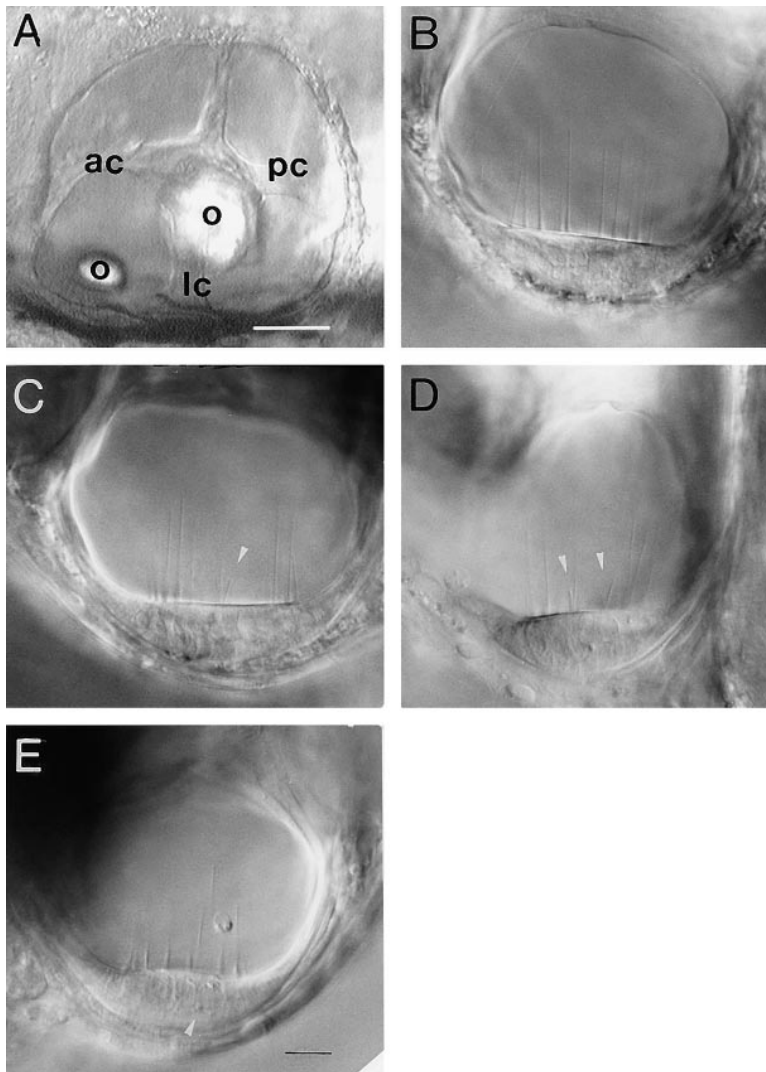
Figure 4. Gross and Fine Anatomy of the Inner Ear In Vivo

(A) Lateral view of the canal structures and otoliths in a wild-type larva at 120 hr. The plane of focus is of the epithelial columns that divide the endolymph-filled space of the otocyst into orthogonally arranged anterior (ac), lateral (lc), and posterior (pc) canals. The stone-like otoliths (o) are oriented at perpendicular angles to one another and are coupled to an underlying patch of sensory hair cells via an otolithic membrane. Scale bar, 40 μm.

(B) Dorsal view of a wild-type crista (sensory hair cell patch) within a semicircular canal at 120 hr using Nomarski differential interference contrast optics. The plane of focus in each panel includes only a portion of the hair cells. Wild-type hair cell bundles are rigid, and the stereociliary bundles are tightly linked and tapered.

(C) Dorsal view of a *mariner* crista at 120 hr. The white arrow indicates stereocilia that are detached from the kinocilium and no longer linked to each other (allele *tc320b*). A similar detachment defect was also seen in *sputnik* cristae.

(D) Dorsal view of a *sputnik* crista at 120 hr. The white arrows indicate two stereociliary bundles that are partially or completely detached from their respective kinocilia (allele *tz300a*). A similar splaying defect was also seen in *mariner* cristae.

(E) Dorsal view of a *skylab* crista at 120 hr. A floating body with a presumptive nucleus is present near the kinocilia. Large round cells are visible within the neuroepithelium (the white arrow indicates a swelling cell with an abnormally visible organelle, most likely the nucleus).

Scale bar, 10 μm.

splayed or detached from each other. The allele strength differs among both *mariner* and *sputnik*. In mutant *mariner* larvae carrying the *tc320b* allele, 36% of hair bundles were splayed (80 bundles, n = 12 larvae). A similar percentage of splayed bundles was seen in *ty220d* larvae (26%; 113 bundles, n = 8 larvae), whereas in *tr202b* larvae, only 5% were splayed (139 bundles, n = 14 larvae). The *tc317e* and *tc242b* alleles of *sputnik* are of approximately equal strength, causing a splayed phenotype in 50%–53% of the hair bundles (>108 bundles each, n > 12 larvae each), whereas in *tz300a* larvae, 14% were splayed (92 bundles, n = 12; the *tj264* allele is unavailable) and in *te370e* larvae carrying the weakest allele of *sputnik*, only 1.4% were splayed (206 bundles, n = 12). In addition, we found a different type of defect, degeneration of the neuroepithelia, in *skylab* larvae (Figure 4E, n = 10). Blebs or membranous swellings occurred at the apical surface of the neuroepithelium, and floating bodies were found near the kinocilia. Large, round cells, presumably dying hair cells, were also found within the neuroepithelium. Bundle morphology in *skylab* larvae appeared normal. In the mutants of the other

circler genes, *mercury, orbiter, gemini, astronaut*, and *cosmonaut*, no abnormalities could be detected in the hair cell bundles and epithelium (n = 10 or more per allele; data not shown). However, in all mutants, with the exception of *cosmonaut*, we found tiny pieces of cellular debris floating in the semicircular canals in many of the larvae (>60%) and occasionally a round cell was seen in the neuroepithelia. Cellular debris was also found in wild-type fish of the same age, but at a lower frequency (25%; n = 20).

In addition, we examined the lateral line organ of each mutant with a fluorescent dye, DASPEI (2-[4-dimethyl-aminostyryl]-N-ethyl pyridinium iodide), which stains the sensory hair cell bodies. The larval lateral line organ consists of 50 or more neuromasts or sensory patches of 8–16 hair cells, which are located on the head and trunk in a stereotypical pattern. The hair bundles protrude directly into the surrounding swimming water, and are covered only by an acellular, gelatinous cupula that enables an efficient viscous-elastic coupling to the surrounding fluid. The organ serves both as a proprioceptor to detect the propulsion of the body in the water and
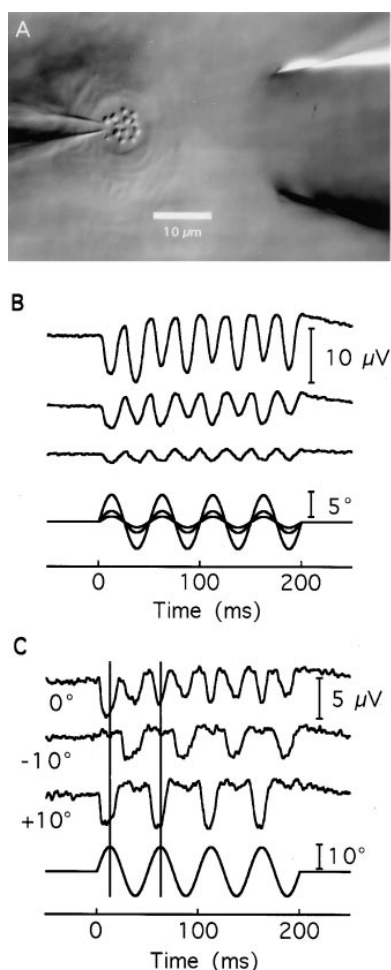
Figure 5. Microphonic Potentials in Lateral Line Neuromasts in Wild-Type Zebrafish Larvae

(A) Top view of a lateral line neuromast on the tail of a 6-day-old wild-type animal during mechanical stimulation with a fluid jet delivered by the large micropipette on the right. A small micropipette on the left was carefully placed at the periphery of the group of hair bundles of this neuromast and used as a voltage-sensing electrode. Individual hair bundles are visible as triangular structures with a faint white dot, the kinocilium, on one side indicating the orientation of the bundles. Seven hair bundles face the voltage-sensing electrode, while the remaining five hair bundles face in the opposite direction. The relief-like structures in the background are skin cells. The cupula is out of focus above this optical section.

(B) Family of voltage responses to a series of mechanical deflections of increasing amplitudes. The cupula and hair bundles were deflected by a stiff glass probe that was attached to a piezo bimorph and driven by a sinusoidal voltage (20 Hz, 4 cycles). Note that the response has twice the frequency of the mechanical stimulus. Traces are averages of 200 presentations.

(C) Microphonics of another neuromast during saturating deflections with a stiff glass probe and superimposed bias deflections of ±10°.
(Top trace) The neuromast doubles the stimulus frequency when the hair bundles are stimulated from their resting position.
(Upper middle trace) Hair bundles were deflected by −10° toward the tail end of the fish to saturate one group of the neuromast hair cells in their inhibitory direction. Note that the microphonics have the same frequency as the stimulus.
(Lower middle trace) A biasing deflection of +10° saturated the opposing group of hair cells. Note that the response is shifted by 180°, indicated by the vertical lines.
(Bottom trace) Stimulus protocol. Averages of 60 presentations.

as an exteroceptor to detect water-borne mechanical stimuli (Popper and Platt, 1993). We examined DASPEI-stained neuromasts in all of the mutants and found no differences in the stereotypical pattern of the lateral line (data not shown). However, there were some significant differences in the number of hair cells per neuromast. The average number of hair cells per wild-type neuromast was 10.4 ± 1.9 (n = 27), whereas in mutant *skylab* larvae that undergo neuroepithelial degeneration, the mean was 5.8 ± 1.1 (n = 22; two-tailed t test; P = 0.0001). The mutant *mercury* also had a slightly lower number of hair cells with a mean of 8.9 ± 1.2 hair cells per neuromast (n = 21; P = 0.0026). The other mutants did not show a significant decrease in the number of hair cells per neuromast (data not shown).

Microphonics of Lateral Line Hair Cells

In several mutants, no obvious morphological defects of the hair cells could be found despite the obvious behavioral defects, so we performed extracellular recordings of their mechanosensory function. Since the larval lateral line organ contains mechanosensory hair cells that are located superficially and are therefore readily accessible, we measured the extracellular voltage responses, the microphonic potentials, of lateral line neuromasts (reviewed by Flock, 1965).

Microphonic potentials are generated because current enters the hair cells through the mechanically activated transduction channels at the tip of the hair bundle and leaves the cell through its basolateral membrane. The electrical current loops and the corresponding electrical field lines spread out extracellularly over several micrometers (see below). The spreading occurs because tight junctions insulate the basolateral from the apical electrolyte compartment. We measured this extracellular voltage drop by placing a voltage-sensing microelectrode between the hair bundles of a neuromast as shown in Figure 5A. Because the hair bundles of a neuromast are closely grouped together in a disk-like opening of the skin, all bundles lie roughly within one electrical length constant of the neuromast ($\sim$5 μm; see below). Therefore, hair bundles on the opposite side of the neuromast still make a significant contribution to the microphonic potentials of a neuromast even when the voltage electrode is located eccentrically (Figures 5A and 5B).

The hair bundles are covered by a gelatinous cupula which we deflected either with a stiff glass probe or a fluid jet. In wild-type larvae, the microphonics increased in size with increasing deflections until the response saturated for deflections of about 5° or larger at 15.4 ± 4.1 μV, measured peak to peak (Figure 5B; n = 4). In the remainder of the experiments, we examined the saturating responses to a fluid jet (Figure 5A) and obtained a similar value of 17.0 ± 6.4 μV (Table 2; n = 9).

Although these lateral line responses are minute voltages that could be measured only after intensive averaging, the following observations provide strong evidence that they are caused by the hair cells and are not an experimental artifact. First, the voltage responses were maximal when measured in between the hair bundles of a neuromast and decreased exponentially with a mean

length constant of 5.2 $\pm$ 1.3 μm when the recording electrode was laterally withdrawn during mechanical stimulation (n = 4). Fifty micrometers away from the neuromast, no voltage change was recorded. Secondly, the voltage responses had twice the stimulus frequency (Figure 5B). This was expected, as the hair cells of the neuromast form two groups with opposing orientations of their hair bundles (Figure 5A; Flock and Wersäll, 1962). Furthermore, strong mechanical biases of $\pm$10° could eliminate one of the two frequency components (Figure 5C; Flock, 1965), further emphasizing the physiological origin of the microphonics. Thirdly, the microphonics were completely but reversibly suppressed when 1 mM amiloride or 1 mM dihydrostreptomycin was added to the extracellular solution (data not shown). Both amiloride and streptomycin are known blockers of the mechanoelectrical transduction channel (Jørgensen and Ohmori, 1988; Kroese et al., 1989).

Microphonics of the Mutants

We measured the microphonics of mutant neuromasts (120 hr) directly after and before identical control measurements in wild-type animals (Table 2). During microphonic recordings, particular care was taken to select only neuromasts with intact hair bundles. The microphonics were completely absent in mutant *mercury* larvae and in mutant larvae carrying the strongest alleles of *orbiter*, *sputnik*, and *mariner*. Reductions in microphonic amplitude by $\sim$65% or more were seen in mutant *gemini* larvae, as well as mutant larvae carrying weaker alleles of *sputnik*, *mariner*, and *orbiter*. In the case of the weaker *sputnik* allele, *te170e*, we observed either reductions or the complete absence of microphonic potentials. Seven out of 10 *te370e* neuromasts produced small microphonics of 5.5 $\pm$ 1.6 μV (peak to peak; deflections $\geq$5°; Table 2). This is about one-third of the amplitude of the wild-type microphonics. Three other *te370e* neuromasts had no clear response that could be distinguished from noise. In mutant *astronaut* and *cosmonaut* larvae, the microphonics were similar to wild type, although the signals were slightly lower in *astronaut* larvae. We did not measure the microphonics in *skylab* larvae, since the majority of their neuromasts had only one to three hair bundles left that showed signs of swelling and morphological alterations.

A partial reduction of the microphonics could be caused by a degeneration or lack of tight junctions between hair cells and supporting cells of the neuromast sensory epithelium. A lack of tight junctions would decrease the electrical length constant and potentially reduce the magnitude of the microphonics that can be picked up by a microelectrode. We therefore measured the electrical length constant in mutant *orbiter* (*tc256e* allele), *gemini* (*tc323d* allele), and *astronaut* (*tm290d* allele) larvae that have reduced microphonics. The spatial distribution of the microphonics was similar to that of wild-type larvae (wild-type, 5.2 $\pm$ 1.3 μm; *orbiter*, 5.8 $\pm$ 1.3 μm, n = 3; *gemini*, 4.7 $\pm$ 1.0 μm, n = 3; *astronaut*, 4.8 $\pm$ 1.7 μm, n = 4). Thus, we can rule out that these mutations affect the tight junctions of the sensory epithelium.

The absence of microphonic potentials could be caused

by specific defects of the mechanoelectrical transduction apparatus as well as by general defects of the hair cell, such as an abnormal resting membrane potential. Indeed, the resting potential provides the driving force of the transduction current. We therefore made whole-cell patch-clamp recordings of wild-type and *mercury*, *orbiter*, *sputnik*, and *mariner* larvae that lacked microphonic potentials. Wild-type hair cells had an average resting membrane potential of -61.7 $\pm$ 5.0 mV (n = 7). *mercury* (*tk256c* allele) hair cells had a potential of $-$60.5 $\pm$ 4.4 (n = 4); *sputnik* (*tz300a* allele) hair cells had a potential of $-$67 $\pm$ 6.4 mV (n = 6); *orbiter* (*th263b* allele) hair cells had a potential of $-$66 $\pm$ 11 (n = 2); and *mariner* (*tc320b* allele) hair cells had a potential of $-$63 $\pm$ 15.6 (n = 2). The mean potential of each mutant is within the range obtained for wild type. These whole-cell recordings indicate that the defects in mutant hair cells are not due to an absence of driving force for the transduction current. On the basis of these data, we conclude that those mutants with normal morphology such as *mercury*, *orbiter*, and *gemini*, may have defects that affect an integral molecular component of the transduction apparatus.

Discussion

Based on analysis of behavior, anatomy, and physiology, we can distinguish five classes of zebrafish vestibular mutants. Each class appears to affect auditory-vestibular mechanosensation at a different step. Since complementation analysis of the mutants identifies eight genes, some classes are represented by more than one gene.

Viable alleles of two mutants, *sputnik* and *orbiter*, enabled us to examine adult behaviors associated with equilibrium orientation defects. The dorsal light reflex is a functional test of the otolithic or macular organs that contain low frequency receptors that detect static changes or linear acceleration (reviewed by Pfeiffer, 1964; Popper and Platt, 1993). This reflex is potentiated in *sputnik* and *orbiter* fish, indicative of the presence of a defect within the maculae. The role of larval maculae in balance was also established by analysis of zebrafish mutants, like *keinstein* and *einstein*, in which one or both otoliths are absent (Whitfield et al., 1996). Mutant *keinstein* and *einstein* larvae also swim upside down or sideways in a manner similar to the circlers.

Both vestibular defects and lack of an acoustic-vibrational startle reflex seen in the zebrafish circlers are indicative of a defect in the octavolateralis system. However, these abnormal behaviors may also be due to a defect in the neural circuitry involved in these responses and/or the central nervous system. In fish, the giant reticulospinal Mauthner neurons along with homologous interneurons mediate escape responses evoked by either touch or acoustic-vibrational stimuli (reviewed by Korn and Faber, 1996). Imaging of calcium transients in the larval Mauthner neurons and additional interneurons of the midbrain and hindbrain after tactile stimulation demonstrates that these reticulospinal neurons are normal in mutant circler larvae. In contrast to experiments with wild-type larvae, we observed no or strongly reduced changes in neuronal calcium concentration upon

vibrational stimulation of mutant larvae with the exception of *skylab* and *cosmonaut*. The vibrational stimulus presumably activates sensory hair cells, which in turn activate first-order neurons of the eighth nerve ganglion that synapse with the Mauthner neurons (reviewed by Korn and Faber, 1996). The lack of this reflex or reduction in response strongly suggests that the defects in the circlers are peripheral.

Upon close examination of the sensory neuroepithelia, two types of hair cell defects were found: bundle integrity defects and degeneration. Splayed or detached stereocilia were found in two mutants, *sputnik* and *mariner*. Degeneration consisting of round, swollen hair cells and floating membranous debris was found in one mutant, *skylab*. The remaining five mutants had no detectable morphological defects, pointing to the possibility of functional defects. Indeed, measurements of the microphonic or extracellular potentials of lateral line hair cells suggest that the morphologically normal mutants, with the exception of *astronaut* and *cosmonaut*, do not generate receptor potentials.

The physiological analysis of the hair cell microphonics and vibrational-acoustic startle reflex, together with the morphology of the sensory neuroepithelia, permits preliminary classification of the circlers in relation to the sequence of events during mechanotransduction. These events include displacement of the hair cell bundle, mechanoelectrical transduction, and events subsequent to transduction.

Excitation of a hair cell occurs during displacement of its hair bundle toward the kinocilium. The degree of displacement is determined by the stiffness of the bundle, which is dependent upon the elastic properties of the extracellular links between stereocilia (Pickles, 1993). Mutations in *sputnik* and *mariner* appear to affect bundle integrity. Stereociliary bundles can be found detached from their respective kinocilia, and in some cases, the stereocilia are splayed. Microphonic or extracellular potentials were completely absent in the majority of nonviable *sputnik* and *mariner* mutants. However, those mutants with 5% or less bundle detachment were able to generate a weak microphonic response. Loss of sensitivity to mechanical stimulation may be due to changes within the uppermost extracellular linkages (Jacobs and Hudspeth, 1990; Assad et al., 1990), especially tip links, which are proposed to directly interact with the transducing channels. Since the bundles appear to be mostly intact and yet insensitive, the extracellular linkages may be too relaxed or weak to provide the stiffness necessary for mechanotransduction. This may be due to a defect in the proteins comprising the links or in components that anchor the links to the sites of attachment.

A second group of mutants that includes *orbiter*, *mercury*, and *gemini*, appears to affect the transduction event itself. These mutants also lack microphonic potentials like mutant *sputnik* and *mariner* larvae, but do not have any obvious morphological defects within the sensory epithelium. In addition, the driving force of transduction, the resting membrane potential, is normal in all three mutants. Since the flux of cations through the mechanoelectrical transduction channel is primarily responsible for the microphonics, a lack thereof suggests

a defect in the transduction apparatus. The work on the touch receptor of *C. elegans* (reviewed by Tavernarakis and Driscoll, 1997) highlights the emerging consensus that the transduction machinery of vertebrate and invertebrate mechanoreceptors is likely to be a complex structure of extra- and intracellular components that are intricately coupled to one or several transmembrane elements, including the pore-forming part of the transduction channel. This view is readily supported by the gating-spring model of mechanoelectrical transduction in hair cells (reviewed by Hudspeth and Gillespie, 1994; Hamill and McBride, 1996). The biophysically derived model of the transduction apparatus consists minimally of an extracellular filament, the so-called tip link, the transmembrane transduction channel, and complex intracellular cytoskeletal machinery attached to the stiff actin core of the sterocilia. Therefore, the *orbiter*, *mercury*, or *gemini* genes may encode any one of these elements. Further physiological analysis will be needed to distinguish between these possibilities.

The remaining three classes contain one gene each. Mutant *astronaut* larvae have a greatly reduced response to vibrational stimuli and yet have only slightly reduced microphonics. The *astronaut* gene may therefore be required for receptor potential generation or synaptic transmission at the basal membrane of sensory hair cells. Mutant *cosmonaut* larvae, in contrast to other circlers, are normal in all aspects except for equilibrium orientation and a reduced response to vibrational stimuli. The mutation in *cosmonaut* may also affect events following mechanotransduction like synaptic transmission in hair cells or primary neurons within the eighth nerve. Since the defects in *cosmonaut* and *astronaut* fish appear to be downstream of mechanotransduction, we examined serial sections of the CNS and the morphology of the eighth nerve with a fluorescent dye. No differences were seen between wild-type larvae and *cosmonaut* and *astronaut* mutant larvae (data not shown). The last class contains *skylab*, the only mutant that shows a significant degree of degeneration of the sensory neuroepithelium. The *skylab* gene product may therefore be involved in the maintenance or survival of hair cells.

Although the classification of the circlers is putative and limited by the number of available alleles, these zebrafish mutants offer the oppurtunity to dissect genetically the phenomenon of sensory hair cell transduction. Characterization of the circler genes will complement biophysical studies and thus advance our understanding of the molecular basis of auditory transduction. In addition, zebrafish mutants with defects similar to those seen in human hereditary forms of deafness may serve as informative models for such disorders, since zebrafish larvae are accessible to a wide range and level of analyses as shown here.

Experimental Procedures

Fish Maintenance and Breeding
Fish were raised and crossed as described (Mullins, et al. 1994). Identified heterozygous carriers in a Tübingen background or a background mix of Tübingen and Top Long fin (Haffter et al., 1996) were crossed to each other to identify alleles of each gene (Table 1). Mutations were scored as noncomplementing or allelic if 25%

of the progeny from a complementation cross had vestibular defects and, depending on the cross, were insensitive to vibrational stimuli. In all cases, progeny of fish carrying allelic mutations had a phenotype that was similar, if not identical, to homozygous fish. Crosses between heterozygous fish carrying weak and strong alleles resulted in progeny with the stronger phenotype. For example, progeny from a cross of a heterozygous fish carrying the *te370e* mutation and a heterozygous fish carrying the *tc317e* mutation had vestibular defects and were vibration insensitive like *tc317e* homozygous fish.

Embryos were raised at 30°C in E3 medium (containing in mM: 5 NaCl, 0.17 KCl, 0.33 $CaCl_2$, and 0.33 $MgSO_4$) in petri dishes as described (Haffter et al., 1996). In all experiments, wild-type fish are the phenotypically wild-type siblings of the homozygous mutants.

Behavioral Test of the Dorsal Light Reflex

Juvenile or adult fish (older than 1 month) were placed in a 2 l plastic container in a dark room. A spot lamp was positioned at a 90° angle 10 cm away from the container. Fish were kept in total darkness for 1 min in an attempt to eliminate visual cues and then photos were taken within 1–5 min during unilateral illumination.

Microscopy

Live larvae were anesthetized with 0.02% MESAB (3-aminobenzoic acid ethyl ester) and mounted in 3% methyl cellulose in a depression slide. Nomarski differential interference contrast optics were used to visualize the structure of the inner ear and neuromasts.

Calcium Green-1 Dextran Imaging

Embryos (1–4 cell stage) were injected with 4–6 nl 0.5%–1.0% Calcium Green-1 dextran (10 kDa; molecular probes) in 0.2 M KCl (Cox and Fetcho, 1996). They were allowed to recover in Ringer's solution at 30°C in the dark. Day 5 larvae were prescreened for even labeling of the CNS and head region. At 120 hr, labeling in the nervous system is stronger than in other structures, presumably because the increase in cell volume during development is less pronounced in the neuronal lineage. Larvae were anesthetized with 0.02% MESAB in Ringer's solution and decapitated. Decapitation (removing the swimbladder and trunk) reduced movement within the preparation caused by the circulation, but did not significantly change the stimulus-induced calcium signals in the brain, as verified in pilot experiments with whole larvae. The preparations were mounted in 1.5% low-melting agarose in Ringer's solution. MESAB was then washed out after the agarose had solidified.

The recording chamber consisted of a petri dish that was rigidly mounted on the stage of an inverted fluorescence microscope (Axiovert 100, Zeiss). A coverslip was glued to a hole in the bottom through which the preparation was viewed with a cooled 12 bit CCD camera (PXL, Photometrics) using a 10× (NA 0.3, Zeiss) or 20× (NA 0.5, Zeiss) lens and Zeiss filter set 17 (BP485/FT510/515–565). From above, the preparation was viewed during the experiment with a dissection microscope. The stimuli were delivered by the experimenter and timed relative to image acquisition by a photodiode signaling stimulus onset. The vibration stimulus consisted of five light taps to the petri dish within 2–4 s, mimicking the stimulus used in the behavioral assay to trigger the escape reflex. The touch stimulus was delivered to the forehead between the eyes with a micropipette held by a fine remote-controlled micromanipulator. Upon the stimulus signal, the micropipette was quickly driven forward and backward again with the fine control of the manipulator to touch the preparation once.

Series of images (128 × 128 pixel, two frames/s; usually 28 images per series) were acquired with the cooled 12 bit CCD camera in the frame transfer mode. False-color images display the percentage change in fluorescence after stimulus onset relative to the fluorescence immediately before stimulus onset in each pixel. They were obtained from averages over two to four frames before and after stimulus onset. In some cases, when the preparation showed pronounced twitching, the first frame after stimulus onset was omitted from the analysis to exclude motion artifacts. No further corrections were made for bleaching since bleaching was small compared to signal size.

Potential problems with the semi-intact preparation used were artifacts caused by motion of the preparation. In most cases, such motion artifacts were effectively prevented by embedding the preparation in agarose (see also O'Malley et al., 1996), as can be clearly seen in experiments in which the stimulus elicited no calcium signal (*sputnik* larvae and vibrational stimuli; Figure 3F). When stimulation elicited muscle contractions, fast twitches sometimes occurred despite the agarose embedding. In some cases, these artifacts could be reduced by excluding the first frame after stimulus onset during which twitching occurred (see O'Malley et al., 1996). Moreover, in the regions of interest here (the ear and the brain) movement artifacts were usually small or absent, which is evident from preparations that did not respond to each stimulus with a strong twitch. However, trials in which significant movement artifacts were observed were excluded from quantitative analysis. To facilitate comparison of mean peak signals, the mean wild-type value (2.4% ΔF/F) was set to 100%.

Microphonic and Whole-Cell Recordings

Day 5 larvae were anesthetized with 0.02% MESAB in normal extracellular solution and decapitated. Lying on one side, the tails of the larvae were secured with fine glass fibers at the bottom of an experimental chamber. The chamber was constantly superfused at a rate of 20 ml/hr with normal extracellular solution (containing in mM: 120 NaCl, 2 KCl, 2 $CaCl_2$, and 10 HEPES [pH 7.3]). Tetrodotoxin (100 nM) was added to suppress muscle twitching and provide more stable recording conditions. Hair cells were visualized with an upright microscope (Zeiss Axioskop, Oberkochen, Germany) equipped with Nomarski differential interference contrast optics, a 40× water immersion objective, and a video contrast enhancement system (Hamamatsu, Japan). Because of the excellent transparency of the tail part of the animal, most experiments were done on the last two neuromasts on the tail end of the fish.

Mechanical Stimulation

Mechanical stimulation of the lateral line hair cells was done by deflecting the cupula of the neuromast either with a piezo-driven water jet or a stiff glass probe attached to a piezo bimorph. In both cases sinusoidal command signals of between 1 and 50 Hz were used; however, most recordings were done with a 20 or 40 Hz stimulus command.

For the water-jet stimulation, a glass micropipette (tip diameter, 50–100 μm) was placed parallel to the long body axis ∼100 μm away from the neuromast. This method of stimulation can be set up quickly and allows for a speedy test of the lateral line microphonics. However, exact calibration of the water-jet stimulus is difficult and time consuming. Instead, displacements of the hair bundles were evaluated by eye on the video screen, and the stimulus command was adjusted to ensure saturating deflections of ≥5°. We used the voltage driving the water-jet stimulator as a measure of displacement.

For a more quantitative stimulation of the hair bundles, we mounted a glass micropipette on a piezo-bimorph element to deflect it parallel to the plane of focus. Twenty to twenty-five micrometers above the cell surface at the height of the tips of the kinocilia, the cupula of the neuromast was partially drawn into the micropipette (tip diameter, 5 μm). Movements of the cupula and attached hair bundles were observed on the video screen and seen to follow the lateral displacements of the pipette precisely. Lateral displacements were linearly related to the driver voltage put across the piezo bimorph. The movement of the pipette was calibrated against a micrometer scale.

The linear displacement, d, of the cupula at the tips of the kinocilia was transformed into an angular deflection, α, expressed in degrees, according to the equation: $\alpha = \arcsin(d/h)$, where h is the height of the kinocilia, usually 20–25 μm.

Electrical Recordings

Microphonic potentials were measured with an Axopatch 200B amplifier in current-clamp mode. Voltage signals were further amplified (total amplification, 50,000), filtered at 200 Hz by an eight-pole Bessel filter, and digitized at a sampling rate of 0.2 ms by a 16-bit acquisition board (ITC16, Instrutech, Great Neck, NY) in conjunction with a Power Macintosh 7600/132 computer running lab-written data-aquisition routines. Micropipettes with tip openings between

1 and 5 μm were filled with normal extracellular solution, placed within 1 μm at the base of the hair bundles, and used as voltage-sensing electrodes. Their electrical resistance was between 0.5 and 5 MΩ. Electrodes with a large tip diameter (1–5 μm) and therefore low electrical resistances were chosen to reduce the noise level and to avoid development of tip potentials observed in very fine micropipettes. The tip of the electrode was always placed at the periphery of the hair bundle group, and care was taken that the recording electrode did not touch a bundle or impede mechanical stimulation of the bundles by the water jet. Usually, between 20 and 2100 presentations were averaged.

For the measurements of the electrical length constant, a neuromast was stimulated by saturating deflections from the fluid jet. The microphonics were repeatedly measured with the voltage-sensing electrode placed at increasing distances from the neuromast. The distance from the edge of the neuromast to the tip of the recording pipette was measured from the calibrated video screen. Microphonics were plotted versus the distance from the neuromast, and data were fitted with a single exponential: $A_0 \exp(-x/\tau)$, where x is the distance between recording pipette and the edge of the neuromast, A_0 is the size of the peak-to-peak microphonics at x = 0 μm, and τ is the electrical length constant.

Resting membrane potentials were recorded in whole-cell patch-clamp recordings. Skin cells and most supporting cells covering the neuromast hair cells were mechanically removed with micropipettes so that patch pipettes could seal onto the basolateral membrane of the hair cells. Pipettes were filled with (in mM) 105 KCl, 5 EGTA-KOH, and 5 HEPES (pH 7.4). Their electrical resistances were between 5 and 15 MΩ, of which between 0% and 90% were electronically compensated.

We did not record any transduction currents during these whole-cell recordings. As the limited space around the hair bundle precludes any sealing on the apical membrane, we patched onto the basolateral membrane of the hair cell bodies that were mechanically exposed by removing overlying skin cells with large cleaning micropipettes (tip diameter, 20–30 μm). Since substantial force had to be exerted to tear off the tough and sturdy skin cells, the delicate structures of the nearby hair bundles were regularly compromised and often destroyed. Under these circumstances, partially reduced or totally absent transduction currents in mutant animals would not have been meaningful.

All experiments were done at room temperature (22°C–26°C).

References

Ashmore, J. (1991). The electrophysiology of hair cells. Annu. Rev. Physiol. 53, 465–476.

Assad, J., Shepherd, G., and Corey, D. (1991). Tip-link integrity and mechanical transduction in vertebrate hair cells. Neuron 7, 985–994.

Avraham, K., Hasson, T., Steel, K., Kingsley, D., Russell, L., Mooseker, M., Copeland, N., and Jenkins, J. (1995). The mouse Snell's waltzer deafness gene encodes an unconventional myosin required for structural integrity of inner ear hair cells. Nature Genet. 11, 369–375.

Bagger-Sjöbäck, D., and Wersäll, J. (1973). The sensory hairs and tectorial membrane of the basilar papilla in the lizard Calotes versicolor. J. Neurocyt. 2, 329–350.

Brown, S., and Steel, K. (1994). Genetic deafness—progress with mouse models. Hum. Mol. Gen. 3, 1453–1456.

Corey, D., and Hudspeth, A. (1983). Kinetics of the receptor current in bullfrog saccular hair cells. J. Neurosci. 3, 962–976.

Corwin, J., and Warchol, M. (1991). Auditory hair cells: structure, function, development, and regeneration. Annu. Rev. Neurosci. 14, 301–333.

Cox, K., and Fetcho, J. (1996). Labeling blastomeres with a calcium indicator: a non-invasive method of visualizing neuronal activity in zebrafish. J. Neurosci. Methods 68, 185–191.

Denk, W., Holt, J., Sheperd, G., and Corey, D. (1995). Calcium imaging of single stereocilia in hair cells: localization of transduction channels at both ends of tip links. Neuron 15, 1311–1321.

Driscoll, M., and Chalfie, M. (1991). The mec-4 gene is a member of a family of Caenorhabditis elegans genes that can mutate to induce neuronal degeneration. Nature 349, 588–593.

Du, H., Gu, H., William C., and Chalfie, M. (1996). Extracellular proteins needed for C. elegans mechanosensation. Neuron 16, 183–194.

Flock, Å. (1965). Transducing mechanisms in the lateral line canal organ receptors. Cold Spring Harbor Symp. Quant. Biol. 30, 133–145.

Flock, Å., and Wersäll, J. (1962). A study of the orientation of the sensory hairs of the receptor cells in the lateral line organs of fish, with special reference to the function of the receptors. J. Cell Biol. 15, 19–27.

Gibson, F., Walsh, J., Mburu, P., Varela, A., Brown, K., Antonio, M., Belsel, K., Steel, K., and Brown, S. (1995). A type VII myosin encoded by the mouse deafness gene shaker-1. Nature 374, 62–64.

Gillespie, P. (1995). Molecular machinery of auditory and vestibular transduction. Curr. Biol. 4, 449–455.

Granato, M., van Eeden, F., Schach, U., Trowe, T., Brand, M., Furutani-Seiki, M., Haffter, P., Hammerschmidt, M., Heisenberg, C., Jiang, Y., et al. (1996). Genes controlling and mediating locomotion behavior of the zebrafish embryo and larva. Development 123, 399–413.

Hackney, C. and Furness, D. (1995). Mechanotransduction in vertebrate hair cells: structure and function of the stereociliary bundle. Am. J. Physiol. 268, C1–C13.

Haddon, C. and Lewis, J. (1996). Early ear development in the embryo of the zebrafish, Danio rerio. J. Comp. Neurol. 365, 113–128.

Haffter, P., Granato, M., Brand, M., Mullins, M.C., Hammerschmidt, M., Kane, D.A., Odenthal, J., van Eeden, F.J.M., Jiang, Y.-J., Heisenberg, C.-P., et al. (1996). The identification of genes with unique and essential functions in the development of the zebrafish, Danio rerio. Development 123, 1–36.

Hamill, O., and McBride, D., Jr. (1996). A supramolecular complex underlying touch sensitivity. Trends Neurosci. 19, 258–261.

Howard, J., and Hudspeth, A. (1988). Compliance of the hair bundle associated gating of mechanoelectrical transduction by the bullfrog's saccular hair cell. Neuron 1, 189-199.

Huang, M., and Chalfie, M. (1994). Gene interactions affecting mechanosensory transduction in Caenorhabditis elegans. Nature 367, 467–470.

Huang, M., Gu, G., Ferguson, E., and Chalfie, M. (1995). A stomatin-like protein necessary for mechanosensation in C. elegans. Nature 378, 292–295.

Hudspeth, A. (1989). How the ear's works work. Nature 341, 397–404.

Hudspeth, A., and Gillespie, P. (1994). Pulling springs to tune transduction: adaptation by hair cells. Neuron 12, 1-9.

Jacobs, R., and Hudspeth, A. (1990). Ultrastructural correlates of mechanoelectrical transduction in hair cells of the bullfrog's inner ear. Cold Spring Harbor Symp. Quant. Biol. 55, 547–561.

Jørgensen, F., and Ohmori, H. (1988). Amiloride blocks the mechano-electrical transduction channel of hair cells of the chick. J. Physiol. (Lond.) 3, 577–588.

Kernan, M., Cowan, D., and Zuker, C. (1994). Genetic dissection of mechanosensory transduction: mechanoreception-defective mutations of Drosophilia. Neuron 12, 1195-1206.

Kimmel, C., Patterson, J., and Kimmel, R. (1974). The development and behavioral characteristics of the startle response in the zebrafish. Dev. Psychobiol. 7, 47–60.

Korn, H., and Faber, D. (1996). Escape behavior: brainstem and spinal cord circuitry and function. Curr. Opin. Neurobiol. 6, 826-832.

Kroese, A., Das, A., and Hudspeth, A. (1989). Blockage of the transduction channels of hair cells in the bullfrog's sacculus by aminoglycoside antibiotics. Hear. Res. *37*, 203–218.

Little, K., and Neugebauer, D. (1985). Interconnections between the stereovilli of the fish inner ear. Cell Tissue Res. *242*, 427–432.

Malicki, J., Schier, A., Solnica-Krezel, L., Stemple, D., Neuhauss, S., Stanier, D., Abdelilah, S., Rangini, Z., Zwartkruis, R., and Driever, W. (1996). Mutations affecting the development of the zebrafish ear. Development *123*, 275–283.

Mullins, M., Hammerschmidt, M., Haffter, P., and Nüsslein-Volhard, C. (1994). Large-scale mutagenesis in the zebrafish: in search of genes controlling development in a vertebrate. Curr. Biol. *4*, 189–202.

O'Malley, D., Kao, Y., and Fetcho, J. (1996). Imaging the functional organization of zebrafish hindbrain segments during escape behaviors. Neuron *17*, 1145-1155.

Osborne, M., Comis, S., and Pickles, J. (1984). Morphology and cross-linkage of stereocilia in the guinea-pig labyrinth examined without the use of osmium as a fixative. Cell Tissue Res. *237*, 43–48.

Pfeiffer, W. (1964). Equilibrium orientation in fish. Gen. Exp. Zool. *1*, 77–111.

Pickles, J. (1993). A model for the mechanics of the stereociliar bundle on acousticolateral hair cells. Hear. Res. *68*, 159–172.

Pickles, J., Comis, S., and Osborne, M. (1984). Cross-links between stereocilia in the guinea pig organ of Corti, and their possible relation to sensory transduction. Hear. Res. *15*, 103–112.

Platt, C. (1993). Zebrafish inner ear sensory surfaces are similar to those in goldfish. Hear. Res. *65*, 133-140.

Popper, A., and Platt, C. (1993). Inner ear and lateral line. In The Physiology of Fishes (Boca Raton, FL: CRC Press), pp. 99-136.

Popper, A., Platt, C., and Edds, P. (1992). Evolution of the vertebrate inner ear: an overview of ideas. In Evolutionary Biology of Hearing, D. Webster, R. Fay, and A. Popper, eds. (New York: Springer Verlag), pp. 49–57.

Savage, C., Hamelin, M., Culotti, J., Coulson, A., Albertson, D., and Chalfie, M. (1989). *mec-7* is a β-tubulin gene required for the production of 10-protofilament microtubules in *Caenorhabditis elegans*. Genes Dev. *3*, 870–881.

Tavernarakis, N., Sheffler, W., Wang, S., and Driscoll, M. (1997). unc-8, a DEG/ENaC family member, encodes a subunit of a candidate mechanically gated channel that modulates C. elegans locomotion. Neuron *18*, 107-119.

Thurm, U. (1981). Mechano-electric transduction. Biophys. Struct. Mech. *7*, 245–246.

von Baumgarten, R., Simmonds, R., Boyd, J., and Garriott, O. (1975). Effects of prolonged weightlessness on the swimming pattern of fish aboard Skylab 3. Aviat. Space Environ. Med. *46*, 902–906.

von Holst, E. (1935). Über den Lichtrückenreflex bei Fischen. Publ. Stn. Zool. Napoli *15*, 143–158.

von Holst, E. (1950). Die Arbeitsweise des Statolithenapparates bei Fischen. Z. Vergl. Physiol. *32*, 60–120.

Whitfield, T., Granato, M., van Eeden, F., Schach, U., Brand, M., Furutani-Seiki, M., Haffter, P., Hammerschmidt, M., Heisenberg, C., Jiang, Y., et al. (1996). Mutations affecting development of the zebrafish inner ear and lateral line. Development *123*, 241–254.